Internal deformation of the subducted Nazca slab inferred from seismic anisotropy

Caroline M. Eakin[1,2*], Maureen D. Long[1], Alissa Scire[3], Susan L. Beck[3], Lara S. Wagner[4], George Zandt[3], Hernando Tavera[5]

1. Department of Geology and Geophysics, Yale University, New Haven, Connecticut, USA
2. University of Southampton, National Oceanography Centre, Southampton, UK
3. Department of Geosciences, University of Arizona, Tucson, Arizona, USA
4. Department of Terrestrial Magnetism, Carnegie Institution for Science, Washington, DC, USA
5. Instituto Geofísico del Perú, Lima, Peru
* Corresponding author

Within oceanic lithosphere a fossilised fabric is often preserved originating from the time of plate formation. Such fabric is thought to form at the mid-ocean ridge when olivine crystals align with the direction of plate spreading[1,2]. It is unclear, however, whether this fossil fabric is preserved within slabs during subduction or over-printed by subduction-induced deformation. The alignment of olivine crystals, such as within fossil fabrics, can generate anisotropy that is sensed by passing seismic waves. Seismic anisotropy is therefore a useful tool for investigating the dynamics of subduction zones, but it has so far proven difficult to observe the anisotropic properties of the subducted slab itself. Here we analyse

seismic anisotropy in the subducted Nazca slab beneath Peru and find that the fast direction of seismic wave propagation aligns with the contours of the slab. We use numerical modelling to simulate the olivine fabric created at the mid-ocean ridge, but find it is inconsistent with our observations of seismic anisotropy in the subducted Nazca slab. Instead we find that an orientation of the olivine crystal fast axes aligned parallel to the strike of the slab provides the best fit, consistent with along-strike extension induced by flattening of the slab during subduction[3]. We conclude that the fossil fabric has been overprinted during subduction and that the Nazca slab must therefore be sufficiently weak to undergo internal deformation.

It has long been suggested that the process of seafloor spreading at mid ocean ridges (MOR) induces a lattice preferred orientation (LPO) of olivine in the underlying mantle that is subsequently "frozen-in" to the oceanic plate during its formation[2,3]. For A-type olivine LPO fabrics, typical of dry oceanic lithosphere, the fast *a* axes of olivine tends to align with the plate spreading direction, resulting in a fossilized crystallographic fabric in the oceanic plate[4,5]. Such fossilized fabric will manifest itself as seismic anisotropy, the phenomenon by which seismic wave velocity is directionally dependent. Observations from surface wave derived azimuthal anisotropy[6–8], shear wave splitting[9,10], and refracted P-wave (Pn) velocities[11] all indicate that seismic anisotropy within the oceanic lithosphere is consistent with the concept of fossil spreading.

In subduction zones, where oceanic plates descend into the mantle, it is unclear whether this fossil spreading fabric is preserved within the slab to depth, or if the anisotropic signal is overprinted by subsequent subduction-associated deformation. Observations that directly constrain intra-slab anisotropy are limited in number[12,13], and

47 completely absent for the deep portions of slabs (below 200 km). An alternative model
48 for slab anisotropy invokes vertically aligned, hydrated faults in the upper portion of the
49 slab that result from bending stresses at the outer rise. This phenomenon could result in
50 seismically inferred fast directions that are parallel to the trench, due to a combined SPO
51 (shape preferred orientation) and LPO effect of the serpentinized faults[14], which is
52 consistent with some P-wave and Rayleigh wave observations[14–16] (down to a maximum
53 depth of 200km).

54 The most direct observations of seismic anisotropy usually come from shear wave
55 splitting, whereby the orientation of the fast polarized shear wave (ϕ) and the delay time
56 (δt) between the fast and the slow polarized waves are measured. For most shear wave
57 splitting studies targeting subduction zones, anisotropy within the slab itself is typically
58 disregarded because the relative path length through the slab is small compared to the rest
59 of the upper mantle. For the Nazca slab beneath Peru, however, the unique flat-slab
60 geometry, with a transition from a shallow to steeply dipping slab ~500km inboard from
61 the trench (Figure 1), allowed us to make splitting measurements on the seismic *S* phases
62 with relatively long path lengths through the slab (see Methods), which would normally
63 be difficult to observe. Using data from the PULSE and PeruSE arrays, we obtained 16
64 splitting measurements (out of 36 suitable arrivals) for deep local *S* phases (Figure 2a),
65 with the majority of fast directions oriented approximately N-S (mean ϕ: -6.3), and
66 exhibiting substantial delay times (mean δt: 1.3 s). In the same vicinity as the local *S*
67 results (e.g. area encircled by dashed line in Figure 2a), source-side measurements on
68 downgoing *S* phases measured at distant stations show very similar splitting

characteristics (mean ϕ: -1.2°, mean δt: 1.6 s, number of measurements: 9), suggesting that the two types of phases sample the same anisotropic source region.

Several lines of argument suggest that this main anisotropic source is within the subducting Nazca slab. First, when the raypaths are plotted in 3D (see supplementary information) and compared against the slab outline from regional *S*-wave tomography[18], it is clear that many rays (both local *S* and source-side) have long path lengths through the slab (Figures 2a, S1, S2 and Movie S1). In particular, a cluster of N-S oriented fast splitting measurements towards the center of the study area travel through relatively fast (blue) material all the way from the mid-transition zone (555 km) to the mid-upper mantle (<200 km), representing a total path length of over 250 km through the slab (Figure S1). We also note that this N-S ϕ orientation roughly correlates with the N-S strike of the subducting Nazca plate. Outside of the slab, for measurements that sample mainly sub-slab mantle, the fast directions are generally trench perpendicular (ENE-WSW), most likely reflecting trench normal mantle flow beneath the flat slab[18]. This flow direction is opposite to that previously inferred by less direct *SKS* splitting methods[20], and is discussed in detail in our earlier work[19,21].

Another line of evidence for distinct anisotropy within the slab itself comes from the fact that the most of the local *S* phases arrive ~5-10 seconds earlier than predicted by our reference velocity model (Figure 2b). The *S*-waves must therefore be travelling through relatively fast material with a velocity anomaly on the order of +3.5% (±1.5%) to account for the travel time difference. The magnitude of this required velocity anomaly is comparable with the strength of the velocity anomaly present in the slab (Figure 2a), as estimated from the tomographic inversion[17].

92 Yet another telling observation is the fact that the two slowest local *S* phases,
93 which arrive close to the expected arrival time (see FM05 and FS12 in Figure 2b), exhibit
94 contrasting fast directions (WNW-ESE and NE-SW; green lines in Figure 2a) in
95 comparison to the remainder of the local *S* dataset (~ N-S). When compared against the
96 tomography, the raypaths associated with these two measurements mostly sample outside
97 the slab, especially in the 200-400 km depth range (Figure 2a and S1).

98 Based on the evidence outlined above, we have a group of 23 splitting
99 measurements (14 from local *S* and 9 from source-side teleseismic *S*) that we infer to
100 reflect intra-slab anisotropy (blue bars in Figure 1). The average splitting parameters of
101 this sub-set are -3.4° for ϕ (standard deviation: 27°) and 1.4 s for δt (standard deviation:
102 0.6s). Based on the splitting pattern and the slab geometry, as well as other criteria (see
103 supplementary information), we infer that the main source of anisotropy appears to lie
104 between 200-400 km depth within the slab. Considering this path length of ~200 km
105 through anisotropic material then this would imply an anisotropic strength of ~3-4%,
106 consistent with observations from other subducted slabs[22,23]. When compared to the slab
107 morphology (Figure 1), the fast-axis orientation of these slab splitting results generally
108 appear sub-parallel to the slab contours, with over ¾ of measurements oriented within
109 33° of the slab strike (Figure S3). Because the slab morphology can change abruptly, it is
110 possible that several geometries are sampled along any single raypath, which may
111 account for some of the scatter in the results. In general, however, our inference of ϕ
112 values aligned with the slab strike contrasts with observations of azimuthal anisotropy
113 within the Nazca Plate before it subducts beneath South America[6–8]. These show fast axes

114 sub-parallel to the paleo-spreading direction (roughly E-W), consistent with fossilized A-
115 type (or similar) olivine fabric.

116 In order to quantitatively test the hypothesis that the slab preserves the fossil
117 fabric to depth, we carry out a series of forward models based on likely elastic tensors for
118 the upper mantle (see Methods and supplementary information). For all fabric types
119 considered (olivine A-, B-, C-, and E-type, plus a natural peridotite), the mean angle of
120 misfit between the modeled fast directions and those measured by shear wave splitting
121 (Figure S4) is far greater than the standard observational errors (<20°). This demonstrates
122 that none of the fabric types considered provides a good fit to the data under the
123 assumption of frozen-in anisotropy, suggesting that the fabric frozen within the Nazca
124 Plate must have been overprinted or otherwise modified during subduction.

125 Taking a different approach, we also select the olivine fabric type most likely for
126 dry oceanic lithosphere (A-type)[5] and perform a grid search over all possible 3D rotations
127 to find the orientation (relative to the slab strike and dip) which best predicts our slab
128 splitting results (see supplementary information). Analyzing the top 1% of best-fitting
129 models (Figure S5) reveals a strong clustering of the olivine *a*-axes pointing towards the
130 slab strike (red dots, Figure 3). This best-fit orientation also predicts >3% anisotropy for
131 our raypaths, which can easily reproduce our delay times with reasonable path lengths
132 through the slab (~200km; Figure S6).

133 An alternative explanation for our measurements could invoke the LPO of
134 wasdleyite within the slab at depths below the olivine-to-wadsleyite transition (~410 km).
135 Forward modeling demonstrates that wadsleyite provides an acceptable fit to the data
136 (Figure S7a), but considering the spatial distribution of splitting patterns suggests that the

137 main source of anisotropy is unlikely to be in the transition zone (see Supplementary
138 Information). A third possibility for intra-slab anisotropy could be from SPO-type
139 mechanisms such as aligned serpentinized faults[14]. While shallow hydrous phases such as
140 serpentine will become progressively unstable with increasing pressure, a transformation
141 to DHMS (dense hydrous magnesium silicates)[23] could potentially still contribute to our
142 deep anisotropic source (below 200km). However, this hydrated layer is likely relatively
143 thin, and the predicted faulting geometry is non-optimal for reproducing our splitting
144 observations (supplementary information).

145 Based on our observations and models, it appears likely that the LPO within the
146 subducted lithosphere has been modified by deformation in the upper mantle, with the
147 fast axes of olivine rotated ~90° from the fossil spreading direction (approximately down-
148 dip) to be sub-parallel to the slab strike. This implies either along strike shear or
149 extension in the slab; either scenario would align the fast-axes parallel to the slab strike[5]
150 (the sense of shear is unresolved). Along strike extension is reasonable given the
151 contorted slab morphology and abrupt bends in the contours (Figure 1). This scenario is
152 also supported by T-axes (i.e. the direction of maximum extension) inferred from
153 earthquake focal mechanisms, which also follow the strike of the Nazca slab where it
154 transitions from flat to steep[1].

155 Our inference contrasts with the standard view of slabs as cold, rigid, elastic
156 plates that are strong enough to resist permanent internal deformation and therefore
157 preserve fossil anisotropy to depth. Instead, our results imply that the Nazca slab may
158 deform relatively easily, and may thus be relatively weak. The development of new LPO
159 (and overprinting of previously existing LPO) in particular directly implies plastic

deformation in the dislocation creep regime at relatively large strains. In comparison, simple geometrical estimates of the slab bending strain[25], based on the curvature of the slab contours, have an upper range of $\varepsilon = 1.0\text{-}1.4$ (see Figure S8).

The view of slab deformation suggested by our observations is consistent with some geodynamical modeling; for example, viscous deformation is required to explain the global geoid pattern[26]. The relative amount of viscous versus elastic deformation within slabs is still debated[27,28], perhaps in part because we lack direct observations of the non-elastic strain. Analysis of intra-slab seismic anisotropy such as that described here may therefore provide important new constraints on the deformation and rheology of subducting slabs as they descend through the mantle. A crucial observational limitation, however, lies in the difficulty of isolating the anisotropic signature of the slab. As we found previously in Peru[19,21], standard *SKS* splitting analysis may hint at the presence of intra-slab anisotropy, but cannot constrain it, given that path lengths through the slab are relatively short. It remains to be investigated, therefore, whether other subduction zones display similar modification of the fossilized slab fabric at depth, or if this is unique to the relatively young, warm, and distorted Nazca slab.

References

1. Francis, T. Generation of Seismic Anisotropy in the Upper Mantle along the Mid-Oceanic Ridges. *Nature* **221,** 162–165 (1969).

2. Hess, H. Seismic Anisotropy of the Uppermost Mantle under Oceans. *Nature* **203,** 629–631 (1964).

3. Kumar, A. *et al.* Geometry and state of stress in the central and southern Peruvian flat slab. *Earth Planet. Sci. Lett.* (In Review).

4. Zhang, S. & Karato, S. Lattice preferred orientation of olivine aggregates deformed in simple shear. *Nature* **375,** 774–777 (1995).

5. Karato, S. *Deformation of earth materials. An Introduction to the Rheology of Solid Earth*. (Cambridge University Press, 2008).

6. Maggi, A., Debayle, E., Priestley, K. & Barruol, G. Azimuthal anisotropy of the Pacific region. *Earth Planet. Sci. Lett.* **250,** 53–71 (2006).

7. Debayle, E. & Ricard, Y. Seismic observations of large-scale deformation at the bottom of fast-moving plates. *Earth Planet. Sci. Lett.* **376,** 165–177 (2013).

8. Beghein, C., Yuan, K., Schmerr, N. & Xing, Z. Changes in seismic anisotropy shed light on the nature of the Gutenberg discontinuity. *Science* **343,** 1237–40 (2014).

9. Wolfe, C. & Silver, P. Seismic anisotropy of oceanic upper mantle: Shear wave splitting methodologies and observations. *J. Geophys. Res. Solid Earth* **103,** 749–771 (1998).

10. Harmon, N., Forsyth, D. W., Fischer, K. M. & Webb, S. C. Variations in shear-wave splitting in young Pacific seafloor. *Geophys. Res. Lett.* **31,** (2004).

11. Gaherty, J. B., Lizarralde, D., Collins, J. A., Hirth, G. & Kim, S. Mantle deformation during slow seafloor spreading constrained by observations of seismic anisotropy in the western Atlantic. *Earth Planet. Sci. Lett.* **228,** 255–265 (2004).

12. Audet, P. Seismic anisotropy of subducting oceanic uppermost mantle from fossil spreading. *Geophys. Res. Lett.* **40,** 173–177 (2013).

13. Song, T.-R. A. & Kim, Y. Anisotropic uppermost mantle in young subducted slab underplating Central Mexico. *Nat. Geosci.* **5,** 55–59 (2012).

14. Faccenda, M., Burlini, L., Gerya, T. V. & Mainprice, D. Fault-induced seismic anisotropy by hydration in subducting oceanic plates. *Nature* **455,** 1097–1100 (2008).

15. Eberhart-Phillips, D. & Reyners, M. Three-dimensional distribution of seismic anisotropy in the Hikurangi subduction zone beneath the central North Island, New Zealand. *J. Geophys. Res.* **114,** B06301 (2009).

16. Wagner, L., Fouch, M., James, D. & Long, M. The role of hydrous phases in the formation of trench parallel anisotropy: Evidence from Rayleigh waves in Cascadia. *Geophys. Res. Lett.* **40,** 1–5 (2013).

17. Yu, D. & Wang, L. P-wave anisotropy tomography of central Japan: Insight into subduction dynamics. *Tectonophysics* **592,** 14–30 (2013).

18. Scire, A. *et al.* Imaging the transition from flat to normal subduction: Variations in the structure of the Nazca slab and upper mantle under southern Peru and northwestern Bolivia. *Geophys. J. Int.* (In Revision).

19. Eakin, C. M. & Long, M. D. Complex anisotropy beneath the Peruvian flat slab from frequency-dependent, multiple-phase shear wave splitting analysis. *J. Geophys. Res. Solid Earth* **118,** 4794–4813 (2013).

20. Russo, R. & Silver, P. Trench-Parallel Flow Beneath the Nazca Plate from Seismic Anisotropy. *Science* **263,** 1105–1111 (1994).

21. Eakin, C. M., Long, M. D., Wagner, L. S., Beck, S. L. & Tavera, H. Upper mantle anisotropy beneath Peru from SKS splitting: Constraints on flat slab dynamics and interaction with the Nazca Ridge. *Earth Planet. Sci. Lett.* **412,** 152–162 (2015).

22. Matchem, I., Savage, M. K. & Gledhill, K. R. Distribution of seismic anisotropy in the subduction zone beneath the Wellington region, New Zealand. *Geophys. J. Int.* **140,** 1–10 (2000).

23. Hiramatsu, Y., Ando, M. & Ishikawa, Y. ScS wave splitting of deep earthquakes around Japan. *Geophys. J. Int.* **128,** 409–424 (1997).

24. Faccenda, M. Water in the slab: A trilogy. *Tectonophysics* **614,** 1–30 (2014).

25. Turcotte, D. L. & Schubert, G. *Geodynamics*. (Cambridge University Press, 2002).

26. Hager, B. Subducted Slabs and the Geoid: Constraints on Mantle Rheology and Flow. *J. Geophys. Res. Solid Earth* **89,** 6003–6015 (1984).

27. Farrington, R. J., Moresi, L.-N. & Capitanio, F. A. The role of viscoelasticity in subducting plates. *Geochemistry, Geophys. Geosystems* **15,** 4291–4304 (2014).

28. Fourel, L., Goes, S. & Morra, G. The role of elasticity in slab bending. *Geochemistry, Geophys. Geosystems* **15,** 4507–4525 (2014).

29. Gripp, A. E. & Gordon, R. G. Young tracks of hotspots and current plate velocities. *Geophys. J. Int.* **150,** 321–361 (2002).

30. Müller, R., Sdrolias, M., Gaina, C. & Roest, W. Age, spreading rates, and spreading asymmetry of the world's ocean crust. *Geochemistry, Geophys. Geosystems* **9,** 18–36 (2008).

Corresponding Author

Correspondence and request for materials should be addressed to Caroline M. Eakin at caroline.eakin@gmail.com.

Acknowledgements

The PULSE deployment was facilitated by the PASSCAL program of IRIS (Incorporated Research Institutions for Seismology) and the data was accessed through the IRIS Data Management Center (DMC). We thank all those from Yale University, University of North Carolina – Chapel Hill, University of Arizona and the Instituto Geofísico del Perú (IGP) who participated in the fieldwork. We thank Rob Clayton and Paul Davis for providing access to data from PeruSE stations. We acknowledge helpful discussions and suggestions by Shun Karato on modeling anisotropy within the slab, and thank 3 anonymous reviewers for suggestions that greatly improved the manuscript. The PULSE experiment was supported by National Science Foundation grants EAR-0943962 (MDL), EAR-0944184 (LSW), and EAR-0943991 (SLB).

Author Contributions

C.M.E. conceived the paper topic, made the measurements, and carried out the modeling in collaboration with M.D.L.; A.S. and G.Z. provided the tomographic images and slab

contours; M.D.L., S.L.B., L.S.W., and H.T. were principal investigators on the PULSE deployment; C.M.E. and M.D.L. co-wrote the paper with feedback and input from all co-authors.

Competing Financial Interests

There are no competing financial interests.

Figures

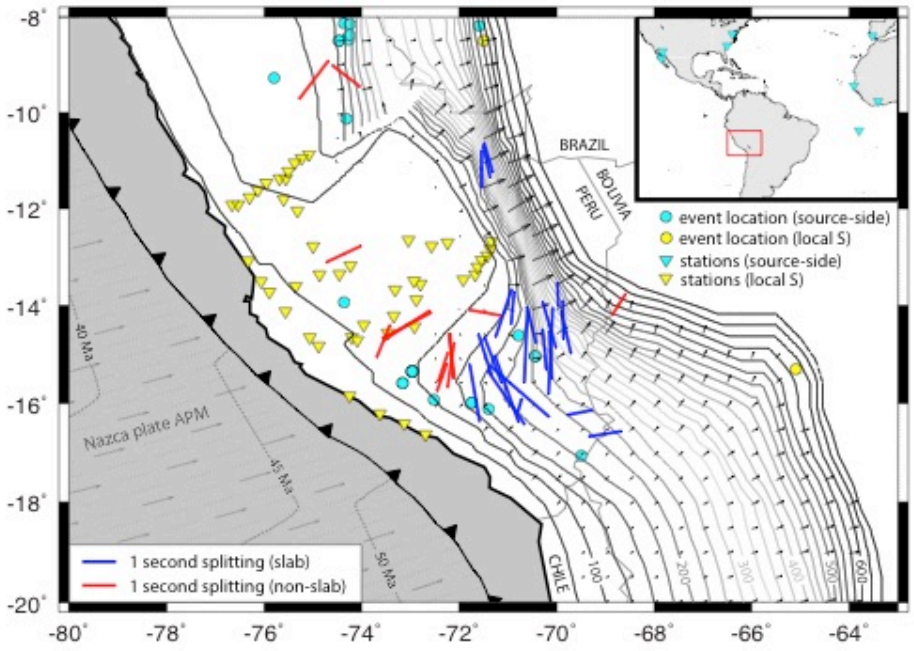

Figure 1. Tectonic setting of southern Peru, showing the distribution of stations and events, and comparing the splitting results with the slab geometry. Slab contours are derived from the regional tomography model and represent the midpoint of the slab at that depth[17]. Black arrows illustrate the slab dip vectors i.e. gradient of the contours. Splitting results (blue and red bars) are plotted at their pierce-point at 300 km depth. The

orientation of the bar represents ϕ, and its length is scaled by δt. Absolute plate motions (APM)[35] and seafloor age contours[36] are shown for the Nazca plate.

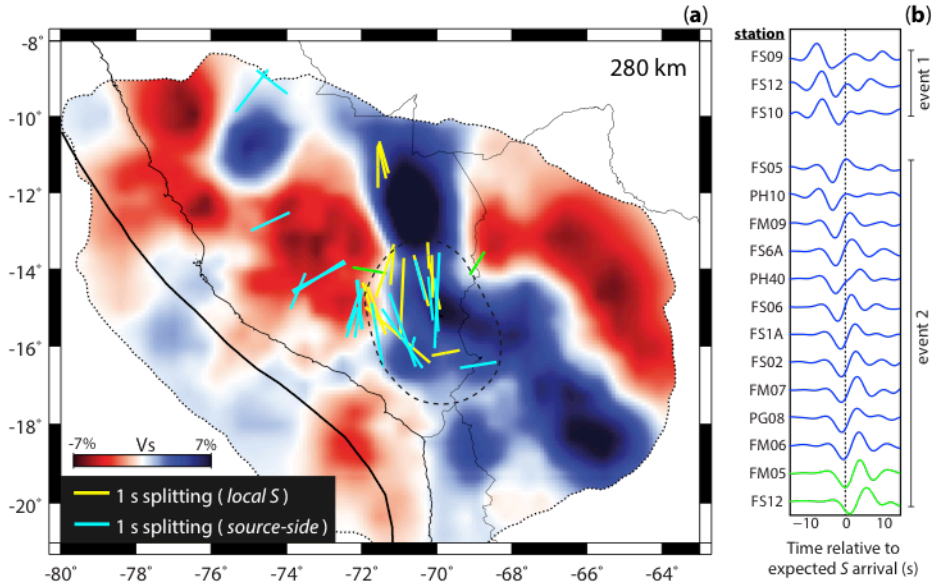

Figure 2. Comparison of the regional splitting pattern with seismic signatures of the subducting slab. (a) Shear wave splitting results overlain on *S*-wave tomography[17]. Splitting measurements are the same as Figure 1. Within the area enclosed by the dashed circle, which overlies the slab (linear dark blue feature), the source-side and local *S* splits show similar characteristics. Two local *S* splits (shown in green) that lie outside the slab show contrasting orientations. (b) Record section of local *S* phases for which splitting was measured. Records are grouped by event and then sorted by arrival time relative to the reference velocity model (Table S1). The normalized horizontal component in the direction of initial polarization is plotted. All seismograms are bandpass filtered from 0.03-0.15 Hz. The two slowest phase arrivals correspond to the green results in sub-figure (a).

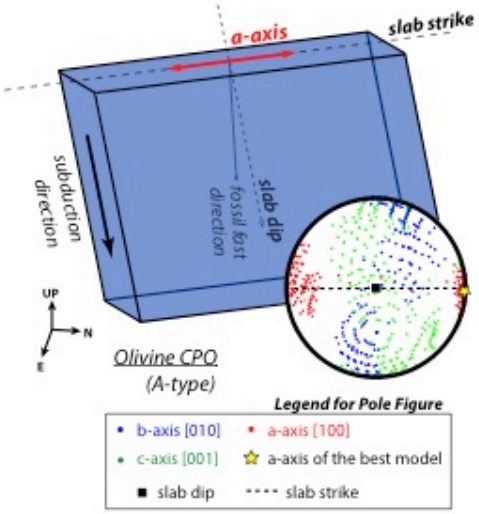

Figure 3. Summary of the modeling results illustrating the orientation of olivine that would best reproduce the slab splitting fast directions. The pole figure (upper hemisphere plotted, looking from above) shows the crystal preferred orientation (CPO) of the main crystal axes (*a*, *b*, and *c*) that would be required by A-type olivine in the upper mantle for the top 1% of models. The similarly slow *b*- and *c*-axes (blue and green dots) are randomly oriented in the symmetry plane, but the fast *a*-axes (red dots) tend to cluster parallel with the slab strike. This favorable *a*-axis orientation is illustrated on the blue cartoon slab.

Methods

Shear Wave Splitting Analysis

We investigated shear wave splitting for local *S* phases originating from deep (> 500 km) events at 40 seismic stations of the PULSE (PerU Lithosphere and Slab Experiment) array, along with 8 stations from the PeruSE (Peru Subduction Experiment)

316 network (Figure 1). Both networks were in operation over a similar ~2.5 year time frame
317 from late 2010 to mid 2013.We searched for deep local events in the global CMT
318 catalogue[31] yielding *S* phases that arrived at the stations with incidence angles less than
319 35°. We found two events that fit this criterion, with moment magnitudes of 5.2 and 6.6,
320 occurring at depths of 533 km and 568 km, respectively (Figure 1). The small number of
321 suitable events is due to the temporary nature of the deployment and the scarcity of deep
322 earthquakes in this area. Local *S* splitting analyses on shallower events (40-170 km) are
323 more abundant and reflect anisotropy above the flat slab[32].

324 Following our previous work[32], we conducted shear wave splitting measurements
325 using the SplitLab software package[33], using the rotation correlation (RC) and eigenvalue
326 (EV) measurement methods for estimating the splitting parameters (ϕ and δt)
327 simultaneously. A variable bandpass filter was applied to all seismograms to improve the
328 signal to noise ratio; the lower cut-off limit of the filter varied from 0.01-0.04 Hz and the
329 upper cut-off from 0.1-0.3 Hz. Quality control procedures followed previous work[32];
330 error estimates were typically less than ±12° in ϕ, and ±0.2 seconds in δt at the 95%
331 confidence level.

332 We integrated our deep local *S* splitting measurements with our previously
333 published source-side splitting dataset[19]. The source-side technique uses direct
334 teleseismic *S* waves originating from local earthquakes in the Nazca slab (event depth
335 range 100-200 km) and measured at distant stations to isolate the contribution from
336 anisotropy beneath the earthquake source, assuming an isotropic lower mantle and
337 applying a correction for upper mantle anisotropy beneath the receiver if needed. Due to
338 this geometrical setup, fast directions measured at the station must be reflected across the

great circle path (i.e. the azimuth) to correct for the down-going versus up-going wave propagation frame of reference. We updated the dataset by adding new splitting measurements from station PVAQ, which, as with stations used previously, displays negligible splitting of *SKS* phases[34] indicating an effectively isotropic upper mantle beneath the station. Teleseismic *S* splitting measurements followed the same procedure used in our previous work[19].

Forward Modeling

We used the Matlab Seismic Anisotropy Toolkit (MSAT)[35] to predict fast splitting directions for a series of elastic tensors that represent different olivine LPO scenarios, along with single-crystal wadsleyite. Each candidate elastic tensor was rotated using the Bunge Euler convention[36] into the candidate orientation. After rotation, we solved the Christoffel equation to predict the orientation of the fast quasi-*S* wave for the ray propagation direction associated with each ray in the shear wave splitting dataset. Fossil spreading scenarios were tested by rotating elastic tensors for various olivine fabric types into an orientation defined by the local slab geometry. The best-fitting A-type olivine fabric orientation was identified by performing a grid search in 10° increments over all possible values for three rotation angles and calculating a mean angular misfit for the entire splitting dataset. Further details of the forward modeling methods and results can be found in the supplementary information.

Data Sources

A compilation of all shear wave splitting measurements presented during this study, including station and event information, is provided as an excel file under the supplementary material section. All the raw seismic data was accessed via the IRIS DMC (Incorporated Research Institutions for Seismology Data Management Center: http://ds.iris.edu/ds/nodes/dmc/). Seismic networks from which data were retrieved include the Global Seismograph Network, the United States National Seismic Network, the Global Telemetered Seismograph Network, GEOSCOPE, the NARS Array, the Portuguese National Seismic Network, the PerU Lithosphere and Slab Experiment and the Peru Subduction Experiment. All seismic data is now publically available.

Code Availability

The SplitLab software package[33] was used to make the shear wave splitting measurements. SplitLab is freely accessible here: http://splitting.gm.univ-montp2.fr/

Modeling of the anisotropic fabrics was performed using the Matlab Seismic Anisotropy Toolkit (MSAT)[35] which can be downloaded from: http://www1.gly.bris.ac.uk/MSAT/

Methods References

31. Ekström, G., Nettles, M. & Dziewoński, A. M. The global CMT project 2004–2010: Centroid-moment tensors for 13,017 earthquakes. *Phys. Earth Planet. Inter.* **200-201,** 1–9 (2012).

32. Eakin, C. M. *et al.* Response of the mantle to flat slab evolution: Insights from local S splitting beneath Peru. *Geophys. Res. Lett.* **41,** 3438–3446 (2014).

33. Wüstefeld, A., Bokelmann, G., Zaroli, C. & Barruol, G. SplitLab: A shear-wave splitting environment in Matlab. *Comput. Geosci.* **34,** 515–528 (2008).

34. Lynner, C. & Long, M. D. Sub-slab seismic anisotropy and mantle flow beneath the Caribbean and Scotia subduction zones: Effects of slab morphology and kinematics. *Earth Planet. Sci. Lett.* **361,** 367–378 (2013).

35. Walker, A. M. & Wookey, J. MSAT—A new toolkit for the analysis of elastic and seismic anisotropy. *Comput. Geosci.* **49,** 81–90 (2012).

36. Bunge, H. J. in *Preferred Orientation in Deformed Metal and Rocks: An Introduction to Modern Texture Analysis* (ed. Wenk, H. R.) 73–108 (Academic Press Inc, 1985). doi:10.1016/B978-0-12-744020-0.50009-2